Mon. Not. R. Astron. Soc. **000**, 000–000 (0000) Printed 2 February 2008 (MN LATEX style file v2.2)

The Effect of Primordial Non–Gaussianity on the Topology of Large-Scale Structure

C. Hikage[1,2⋆], P. Coles[2], M. Grossi[3], L. Moscardini[4,5], K. Dolag[3], E. Branchini[6], S. Matarrese[7,8]

[1] *School of Physics and Astronomy, University of Nottingham, University Park, Nottingham, NG7 2RD*
[2] *School of Physics and Astronomy, Cardiff University, 5, The Parade, Cardiff, CF24 3AA*
[3] *Max-Planck Institut für Astrophysik, Karl-Schwarzschild Strasse 1, D-85748 Garching, Germany*
[4] *Dipartimento di Astronomia, Università di Bologna, via Ranzani 1, I-40127 Bologna, Italy*
[5] *INFN, Sezione di Bologna, viale Berti Pichat 6/2, I-40127 Bologna, Italy*
[6] *Dipartimento di Fisica, Università di Roma TRE, via della Vasca Navale 84, I-40127 Bologna, Italy*
[7] *Dipartimento di Fisica, Università degli Studi di Padova, via Marzolo 8, I-35131, Padova, Italy*
[8] *INFN, Sezione di Padova, via Marzolo 8, I-35131, Padova, Italy*

Accepted 2008 January 10. Submitted 2007 November 19.

ABSTRACT

We study the effect of primordial non–Gaussianity on the development of large-scale cosmic structure using high-resolution N-body simulations. In particular, we focus on the topological properties of the "cosmic web", quantitatively characterized by the Minkowski Functionals, for models with quadratic non-linearities with different values of the usual non–Gaussianity parameter $f_{\rm NL}$. In the weakly non-linear regime (the amplitude of mass density fluctuations $\sigma_0 < 0.1$), we find that analytic formulae derived from perturbation theory agree with the numerical results within a few percent of the amplitude of each MF when $|f_{\rm NL}| < 1000$. In the non-linear regime, the detailed behavior of the MFs as functions of threshold density deviates more strongly from the analytical curves, while the overall amplitude of the primordial non–Gaussian effect remains comparable to the perturbative prediction. When smaller-scale information is included, the influence of primordial non–Gaussianity becomes increasingly significant statistically due to decreasing sample variance. We find that the effect of the primordial non-Gaussianity with $|f_{\rm NL}| = 50$ is comparable to the sample variance of mass density fields with a volume of $0.125(h^{-1}{\rm Gpc})^3$ when they are smoothed by Gaussian filter at a scale of $5h^{-1}$Mpc. The detectability of this effect in actual galaxy surveys will strongly depend upon residual uncertainties in cosmological parameters and galaxy biasing.

Key words: Cosmology: early Universe – large-scale structure of Universe – methods: N-body simulations – analytical – statistical

1 INTRODUCTION

According to the standard scenarios for the formation of large-structure in the Universe, the present-day cosmic density field evolves from small-amplitude initial fluctuations which are described by Gaussian statistics. The hypothesis of primordial Gaussianity is supported by present observations of the Cosmic Microwave Background (CMB), particularly those from the Wilkinson Microwave Anisotropy Probe (WMAP) (Komatsu et al. 2003; Spergel et al. 2007). These results are consistent with an inflationary origin for the primordial perturbations, since the simplest forms of cosmic inflation produce nearly Gaussian fluctuations.

In order to understand the early Universe in more detail, however, it is necessary to measure (or at least constrain) the departures from non–Gaussianity that inevitably arise at some level during the inflationary epoch. For example, the simplest slowly-rolling single field inflation model predicts very small levels of primordial non–Gaussianity, while multi-field inflation models and models with a non-standard kinetic term for the inflation may yield larger effects which could be detected in ongoing or next-generation observations (e.g. Bartolo et al. 2002; Bernardeau & Uzan 2002; Lyth et al. 2003; Dvali et al. 2004; Arkami-Hamed et al. 2004; Alishahiha et al. 2004; Bartolo et al. 2004; Chen et al.

⋆ E-mail: chiaki.hikage@nottingham.ac.uk

2007; Battefeld & Battefeld 2007). Only when such phenomena are detected will it be possible to distinguish between the hundreds of currently viable variations on the theme of inflation by understanding the dynamical behavior of the inflation field.

In order to model the primordial non–Gaussianity that might arise during inflation, the following simple form including quadratic corrections to the curvature perturbation Φ (Bardeen 1980) during the matter era has been often adopted (Gangui et al. 1994; Verde et al. 2000; Komatsu & Spergel 2001):

$$\Phi = \phi + f_{\rm NL}(\phi^2 - \langle\phi^2\rangle), \tag{1}$$

where ϕ represents an auxiliary random-Gaussian field and $f_{\rm NL}$ characterizes the amplitude of a quadratic correction to the curvature perturbations in a dimensionless way. In principle, $f_{\rm NL}$ could be scale-dependent, but current observations are not sufficiently sensitive to detect any such variation, so a constant $f_{\rm NL}$ remains a useful parametrization of the level of non–Gaussianity. Recent analyses of the angular bispectrum for WMAP provides strong constraints on $f_{\rm NL}$ to lie in the range from -54 to 114 at the 95 percent confidence level (Komatsu et al. 2003; Spergel et al. 2007; Creminelli et al. 2006).

The Large-Scale Structure (LSS) of the distribution of galaxies in the Universe provides another potentially powerful probe of primordial non–Gaussianity (Fry & Scherrerd 1994; Chodorowski & Bouchet 1996; Verde et al. 2000; Scoccimarro et al. 2004; Hikage et al. 2006; Sefusatti & Komatsu 2007). The three-dimensional spatial information arising from LSS is potentially a richer source information about primordial non–Gaussianity than the two-dimensional information arising from the CMB. For example, constraints from upcoming cluster surveys should be comparable with current CMB limits and those from galaxy surveys, which could be as tight as $|f_{\rm NL}| \sim 10$ for the planned surveys and $|f_{\rm NL}| \sim 0.2$ for an all-sky survey of galaxies up to redshift $z = 5$ (Sefusatti & Komatsu 2007; Dalal et al. 2007). A variety of large-scale projects of LSS observation covering Gpc^3 volumes are being proposed, such as an extension of the Sloan Digital Sky Survey; APO-LSS survey; The Hobby-Eberly Dark Energy Experiment (HETDEX) (Hill et al. 2004); Wide-Field Multi-Object Spectrograph (WFMOS) (Glazebrook et al. 2005); and the Cosmic Inflation Probe (CIP) mission (Melnick et al. 2004). It is consequently important to study the optimal way to extract information about primordial non–Gaussianity from such surveys.

The statistical analysis of non–Gaussianity has been mainly performed through the calculation of the bispectrum (Verde et al. 2000; Scoccimarro et al. 2004; Sefusatti & Komatsu 2007). Strong motivation for this is that the bispectrum is the simplest statistical function that can measure quadratic non-linearity (e.g. Watts & Coles 2003). Although the quadratic model provides an extremely useful benchmark for statistical analysis techniques, one must always bear in mind that there are many different ways for a random field to be non–Gaussian. In general, there is no one statistic that completely characterizes the statistical nature of a non–Gaussian random field, so a battery of higher-order statistics must be deployed. In particular, when the full nature of non–Gaussianity is virtually unknown, such as is really the case for primordial perturbations, the theoretical model assumed should be validated before its parameters are constrained. Different statistics reflect different aspects of non–Gaussianity so the use of different statistics plays a vital role in this kind of consistency check.

In this paper we use a set of invariant characteristics of the topology of the cosmic web, known as the Minkowski Functionals (MFs). These have already been used to describe the morphological properties of cosmic density fields in a variety of contexts (Mecke et al. 1994; Schmalzing & Buchert 1997; Schmalzing & Górski 1998; Hikage et al. 2003). Four MFs are defined in three-dimensional density fields such as LSS: the volume fraction (V_0); surface area (V_1); mean curvature (V_2); and Euler characteristic (V_3).

Using a perturbative approach, Hikage et al. (2006) derived analytical formulae for the behavior of the MFs for LSS including primordial non–Gaussianity (as a function of $f_{\rm NL}$ as given in equation [1]), in addition to the non–Gaussianity due to non-linear gravity and galaxy biasing. The validity of the perturbative analysis is, however, limited to the weakly non-linear regime. Smaller-scale modes also contain rich information about the primordial density fields, and this could help place more stringent constraints on primordial non–Gaussianity. In this paper, we use high-resolution N-body simulations to study the effect of primordial non–Gaussianity on the MFs from the mildly to strongly non-linear regime. There are two reasons for using the full numerical analysis: one is to see how well the perturbative formulae describe the simulated MFs to check their applicability; the other is to study how the primordial non–Gaussian effect behaves in the strongly non-linear regime and thus to estimate the significance of the effect on the MFs.

The paper is organized as follows. In Section 2, we review the perturbative formulae for the MFs. The details of the N-body simulations and the computing method of the MFs are summarized in Section 3. In Section 4, we compare the perturbative formulae of MFs with simulated results to study the primordial non–Gaussian effect in non-linear regime. Section 5 is devoted to the summary and conclusions.

2 PERTURBATION THEORY

We define the MFs of density fields for a given threshold $\nu \equiv \delta/\sigma_0$, where δ is the density fluctuation, which has zero mean, and $\sigma_0 \equiv \langle\delta^2\rangle^{1/2}$ is its standard deviation. The k-th MF $V_k(\nu)$ can be written separately with the amplitude A_k and the function of ν, $v_k(\nu)$, as

$$V_k(\nu) = A_k v_k(\nu). \tag{2}$$

The amplitude part A_k, which depends only on the power spectrum $P(k,z)$ of the 3-dimensional fluctuation field δ at redshift z, is given by

$$A_k = \frac{1}{(2\pi)^{(k+1)/2}} \frac{\omega_3}{\omega_{3-k}\omega_k} \left(\frac{\sigma_1(z)}{\sqrt{3}\sigma_0(z)}\right)^k, \tag{3}$$

where $\omega_k \equiv \pi^{k/2}/\Gamma(k/2+1)$ gives $\omega_0 = 1$, $\omega_1 = 2$, $\omega_2 = \pi$, and $\omega_3 = 4\pi/3$. The quantity σ_i^2 characterizes the variance

of fluctuating fields for $i = 0$ and that of their derivatives for $i = 1$ given by

$$\sigma_i^2(z) \equiv \int_0^\infty \frac{k^2 dk}{2\pi^2} k^{2i} P(k,z) W^2(kR), \tag{4}$$

where W represents a smoothing kernel. Throughout the paper, we adopt a Gaussian kernel $W^2 = \exp[-(kR)^2]$ where R represents the smoothing scale.

Matsubara (2003) derives the second-order perturbative formulae of the MFs using the multivariate Edgeworth expansion. According to the formulae, the function $v_k(\nu)$ is written with the Gaussian part $v_k^{(\mathrm{G})}$ and the leading part of the non–Gaussian term Δv_k as

$$v_k(\nu) = v_k^{(\mathrm{G})}(\nu) + \Delta v_k(\nu), \tag{5}$$

$$v_k^{(\mathrm{G})}(\nu) = e^{-\nu^2/2} H_{k-1}(\nu), \tag{6}$$

$$\Delta v_k(\nu) = e^{-\nu^2/2} \left[\frac{1}{6} S^{(0)} H_{k+2}(\nu) + \frac{k}{3} S^{(1)} H_k(\nu) + \frac{k(k-1)}{6} S^{(2)} H_{k-2}(\nu) \right] \sigma_0, \tag{7}$$

where $H_n(\nu)$ denote the Hermite polynomials. The leading-order non–Gaussian term $\Delta v_k(\nu)$ is calculated when the three "skewness parameters" $S^{(i)}$ are given.

The three skewness parameters $S^{(i)} (i = 0, 1 \text{ and } 2)$ are computed by integrating the bispectrum $B(k_1, k_2, k_3, z)$ over k_1, k_2, and $\mu \equiv (\mathbf{k}_1 \cdot \mathbf{k}_2)/(k_1 k_2)$ with appropriate weights as (Hikage et al. 2006)

$$S^{(0)}(z) = \frac{1}{8\pi^4 \sigma_0^4(z)} \int_0^\infty dk_1 \int_0^\infty dk_2 \int_{-1}^1 d\mu k_1^2 k_2^2 B(k_1, k_2, k_{12}, z) W(k_1 R) W(k_2 R) W(k_{12} R), \tag{8}$$

$$S^{(1)}(z) = \frac{1}{16\pi^4 \sigma_0^2(z) \sigma_1^2(z)} \int_0^\infty dk_1 \int_0^\infty dk_2 \int_{-1}^1 d\mu k_1^2 k_2^2 (k_1^2 + k_2^2 + \mu k_1 k_2) B(k_1, k_2, k_{12}, z) \times W(k_1 R) W(k_2 R) W(k_{12} R), \tag{9}$$

$$S^{(2)}(z) = \frac{3}{16\pi^4 \sigma_1^4(z)} \int_0^\infty dk_1 \int_0^\infty dk_2 \int_{-1}^1 d\mu k_1^4 k_2^4 (1 - \mu^2) B(k_1, k_2, k_{12}, z) \times W(k_1 R) W(k_2 R) W(k_{12} R), \tag{10}$$

where $k_{12} \equiv |\mathbf{k}_1 + \mathbf{k}_2| = (k_1^2 + k_2^2 + 2\mu k_1 k_2)^{1/2}$.

Throughout this paper, we neglect the non–Gaussianity arising from the non-linearity in relationship between galaxy counts and mass (i.e. galaxy biasing) so as to keep the analysis as simple as possible. The bispectrum B for the matter density fluctuation is then given by

$$B(k_1, k_2, k_3, z) = B_{\mathrm{pri}}(k_1, k_2, k_3, z) + B_{\mathrm{gr}}(k_1, k_2, k_3, z), \tag{11}$$

where B_{pri} and B_{gr} represent the contributions from primordial non–Gaussianity and non-linearity in gravitational clustering respectively:

$$B_{\mathrm{pri}}(k_1, k_2, k_3, z) \equiv \frac{2 f_{\mathrm{NL}}}{D(z)} \left[\frac{P(k_1, z) P(k_2, z) M(k_3)}{M(k_1) M(k_2)} + (\mathrm{cyc.}) \right], \tag{12}$$

$$B_{\mathrm{gr}}(k_1, k_2, k_3, z) \equiv 2 \left[F_2(\mathbf{k}_1, \mathbf{k}_2) P(k_1, z) P(k_2, z) + (\mathrm{cyc.}) \right], \tag{13}$$

where $D(z)$ is the growth rate of linear density fluctuations normalized such that $D(z) \to 1/(1+z)$ during the matter era. The function $M(k)$ and $F_2(\mathbf{k}_1, \mathbf{k}_2)$ are time-independent kernels describing mode-coupling due to non-linear clustering of matter density fluctuations in the weakly non-linear regime. These are given by

$$M(k) \equiv \frac{2}{3} \frac{k^2 T(k)}{\Omega_{\mathrm{m}} H_0^2}, \tag{14}$$

$$F_2(\mathbf{k}_1, \mathbf{k}_2) = \frac{5}{7} + \frac{\mathbf{k}_1 \cdot \mathbf{k}_2}{2 k_1 k_2} \left(\frac{k_1}{k_2} + \frac{k_2}{k_1} \right) + \frac{2}{7} \frac{(\mathbf{k}_1 \cdot \mathbf{k}_2)^2}{k_1^2 k_2^2}. \tag{15}$$

We adopt the linear transfer function $T(k)$ by Eisenstein & Hu (1999). In comparison with numerical simulations, we use the power spectrum of the simulations (the details are explained in the next section) at $z^* = 76.97$ for a theoretical input of the power spectrum $P(k, z^*)$ and then give the power spectrum at z as

$$P(k, z) = \frac{D^2(z)}{D^2(z^*)} P(k, z^*). \tag{16}$$

3 METHODOLOGY

3.1 Numerical Simulations with Primordial Non–Gaussianity

The N-body simulations with primordial non–Gaussianity that we use for this analysis are those described in Grossi et al. (2007). These simulations employ 800^3 dark matter particles in a periodic cubic box with a side length of $0.5h^{-1}$Gpc. The cosmology of our simulations is a flat ΛCDM model with mass density parameter $\Omega_{\mathrm{m}} = 0.3$, baryon density parameter $\Omega_{\mathrm{b}} = 0.04$, Hubble parameter $h = 0.7$, primordial power-law index $n_{\mathrm{s}} = 1$, and $\sigma_8 = 0.9$.

The initial particles are perturbed from an initially homogeneous "glass-like" distribution. The primordial non–Gaussianity is incorporated into a Gaussian-random field with the above cosmology in the form of equation (1). Grossi et al. (2007) explored 7 different scenarios with $f_{\mathrm{NL}} = 0, \pm 100, \pm 500$ and $\pm$ 1000. We have analyzed all of these simulations, but for brevity in this paper we only present results for the Gaussian simulation with $f_{\mathrm{NL}} = 0$ and the two extreme non–Gaussian cases $f_{\mathrm{NL}} = \pm 1000$; results for the other simulations with $f_{\mathrm{NL}} = \pm 100$ are intermediate, as expected.

After Fourier-transforming the primordial non–Gaussian field, the dark matter particles are displaced on the initial grid assuming the Zel'dovich approximation. The simulations are started at $z \approx 100$ and the subsequent gravitational evolution is simulated with the GADGET-2 code (Springel et al. 2005). The Triangular-Shaped Cloud method is used to assign densities onto 512^3 grids. After Fourier-transforming the grid data, we multiply by the Gaussian kernel $\exp[-(kR)^2]$, and then transform them back to real space.

It is instructive first to examine the visual morphology of the clustering pattern. Fig. 1 shows maps of slices of the mass density field with $f_{\mathrm{NL}} = 0$ (middle-row panels) and the relative residuals between $f_{\mathrm{NL}} = \pm 1000$ and $f_{\mathrm{NL}} = 0$ (left and right panels). The residual for the map with $f_{\mathrm{NL}} = x$, $\Delta\rho_x$, is calculated at each pixel as

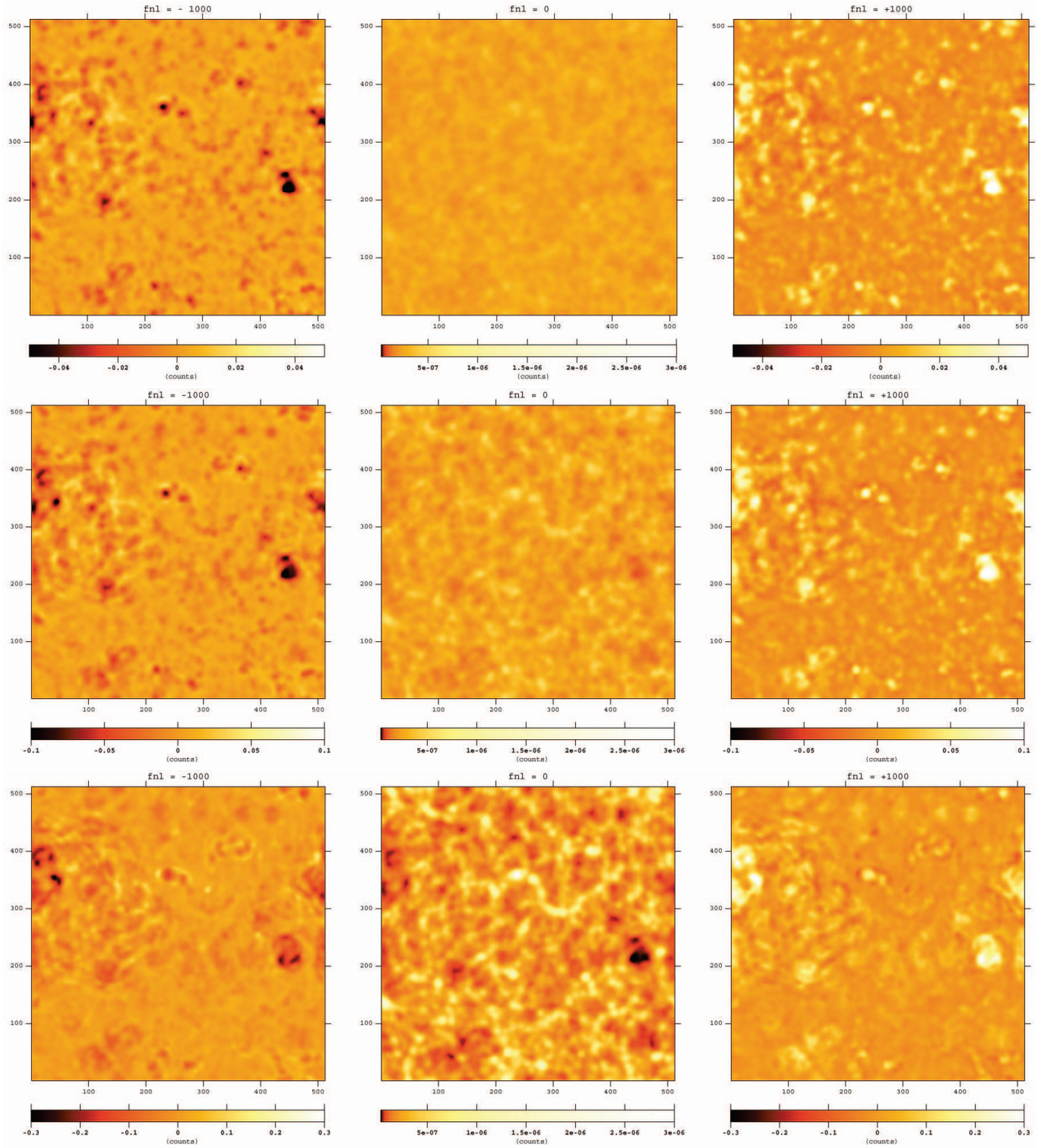

Figure 1. Slice maps of simulated mass density fields at $z = 5.15$ (*top*), $z = 2.13$ (*middle*) and $z = 0$ (*bottom*). The number of pixels at a side length is 512 ($500h^{-1}$Mpc) and that of the thickness is 32 ($31.25h^{-1}$Mpc). The panels in the middle row show the log of the projected density smoothed with a Gaussian filter of 10 pixels width, corresponding to $9.8h^{-1}$Mpc. The left and right panels are the relative residuals for the $f_{\rm NL}$=$\pm$1000 runs (equation [17]). Each panel has the corresponding color bar and the range considered are different from panel to panel.

$$\Delta\rho_x = (\rho_x - \rho_0)/\rho_0 \quad (17)$$

where ρ_x is the number density of mass particles for the map with $f_{\rm NL} = x$. The field is smoothed with a Gaussian filter 10 pixels wide (i.e. $9.8h^{-1}$Mpc). The redshifts of the maps are $5.15, 2.13$ and 0 from top to bottom respectively. Similar density structures in the mass distribution appear in the residual maps with their contrast at same (inverse) sign for positive (negative) values of $f_{\rm NL}$. For example, a large void structure at the right-center in the density map also appears in the residual maps. This is because the higher density region is initially more (less) enhanced in the positive (negative) $f_{\rm NL}$, as predicted by the local model of primordial non–Gaussianity in equation (1).

3.2 Computation of Minkowski Functionals

The computational method we use for calculating MFs of data defined on a grid is based on ideas from integral geometry, rather than the alternative more cumbersome approach of using the differential properties of bounding surfaces. In our case the calculation reduces to counting the numbers of vertices, edges and sides of the elementary cells covering the structure (Coles et al. 1996; Schmalzing & Buchert 1997). The range of ν is from -3.6 to 3.6 with an equal binning width of 0.2. The MFs measured from numerical simulations often deviate from analytical predictions even for Gaussian realizations due to subtle pixelization effects. However, as pointed out by Hikage et al. (2006), pixelization effects become negligible when computing the difference between Gaussian and non–Gaussian MFs. Therefore we focus on $\Delta v_k(\nu_i)$ (i denoting the binning number of ν) that we compute as follows:

(i) We compute the MFs for non–Gaussian simulation data V_k and then divide them by their amplitudes A_k (equation [3]) to obtain normalized MFs v_k. The σ_0 and σ_1 in A_k are computed from the density fields of the simulations.

(ii) The MFs for Gaussian fields are computed in the same way and then divided by their amplitudes A_k where the values of σ_0 and σ_1 are computed from each realization. The same cosmological parameters as the N-body simulations are adopted. The normalized MFs $v_k^{(\rm G)}$ are estimated by averaging MFs over 10 Gaussian realizations.

(iii) The difference ratio Δv_k is computed by

$$\Delta v_k = v_k - v_k^{(\rm G)}. \quad (18)$$

4 RESULTS

In this section we explore two different but related issues. The first is whether the non-linear behaviour seen in numerical simulations matches the predictions of analytical approaches. The second is whether it is possible to separate the effects of non-linear evolution from primordial non-Gaussianity to a sufficient extent for this method to be useful in practice.

4.1 Agreement with perturbative formulae in the weakly non-linear regime

Fig. 2 shows examples of MFs V_k (left panels) and the difference ratio Δv_k (right panels) for simulated mass distributions in the weakly non-linear regime. We smooth on a scale $R = 10h^{-1}$Mpc which, at $z = 3.96$, marks the transition to the non-linear regime since the variance of the smoothed density fluctuation $\sigma_0 \simeq 0.1$. The different symbols show the different $f_{\rm NL}$ of 0 and ±1000. The error-bars represent the sample variance estimated from 1000 Gaussian realizations with the same R, z and box-size as the simulations. The perturbative formulae discussed above are plotted with lines for comparison. Results for the simulations with $f_{\rm NL} = \pm100$ and ±500 are found to be linearly scaled between those with $f_{\rm NL} = 0$ and ±1000.

The theoretical curves reproduce the features of the simulated MFs very well. We quantitatively estimate the agreement between the simulation results $\Delta v_k^{(\rm SIM)}(\nu_i)$ and the perturbative formulae $\Delta v_k^{(\rm PT)}(\nu_i)$ by calculating the root-mean-square (rms) differences averaged over i. Table 1 lists the differences for each MF at different redshifts z (but R is fixed to be $10h^{-1}$Mpc). The differences are less than a few percent relative to the amplitude of each MF (equation [3]) when $\sigma_0 < 0.1$ and remains at the 10-percent level when $\sigma_0 \sim 0.2$. We also estimate the rms differences divided by the rms of $\Delta v_k^{(\rm SIM)}(\nu_i)$ averaged over i. These quantities represent the extent to which the theoretical predictions improve going from linear theory to (2nd-order) perturbation theory. The differences between the 2nd-order perturbative predictions and the numerical simulations is $0.15 \sim 0.41$ times smaller than those corresponding to linear theory at $\sigma_0 < 0.1$. These results are consistent with the previous analysis by Nakagami et al. (2004).

The differences between theory and simulations are quite small compared to the sample variance. However, there is a systematic feature, seen in the asymmetry of V_0 and V_2 with respect to $\nu = 0$; the perturbative predictions are symmetric. There are three possible explanations for this effect. One is that higher-order contributions - i.e. beyond 2nd-order - are significant. Another possibility arises from the use of the Zel'dovich approximation to set the initial conditions of the simulations, which may be responsible for an extra contribution to higher-order statistical properties of clustering arising from transients (Crocce et al. 2006). The other reason is the fact that the multivariate Edgeworth expansion which is the basis of perturbation formulae has a limited range of validity, especially at values of ν larger than unity (Bernardeau & Kofman 1995). These effects must be considered carefully when comparing with real survey results.

4.2 Non-linear evolution and primordial non–Gaussianity

In Fig. 3, we focus on the differences between Δv_k with $f_{\rm NL} = 1000$ and that with $f_{\rm NL} = 0$ at $z = 0$. The perturbative predictions are also plotted for comparison. The deviation from the perturbative predictions becomes significant as the smoothing scale R is smaller (σ_0 increases) due to the primordial non-Gaussian effect coupled with non-linear gravity. The increase of deviations at larger σ_0 are

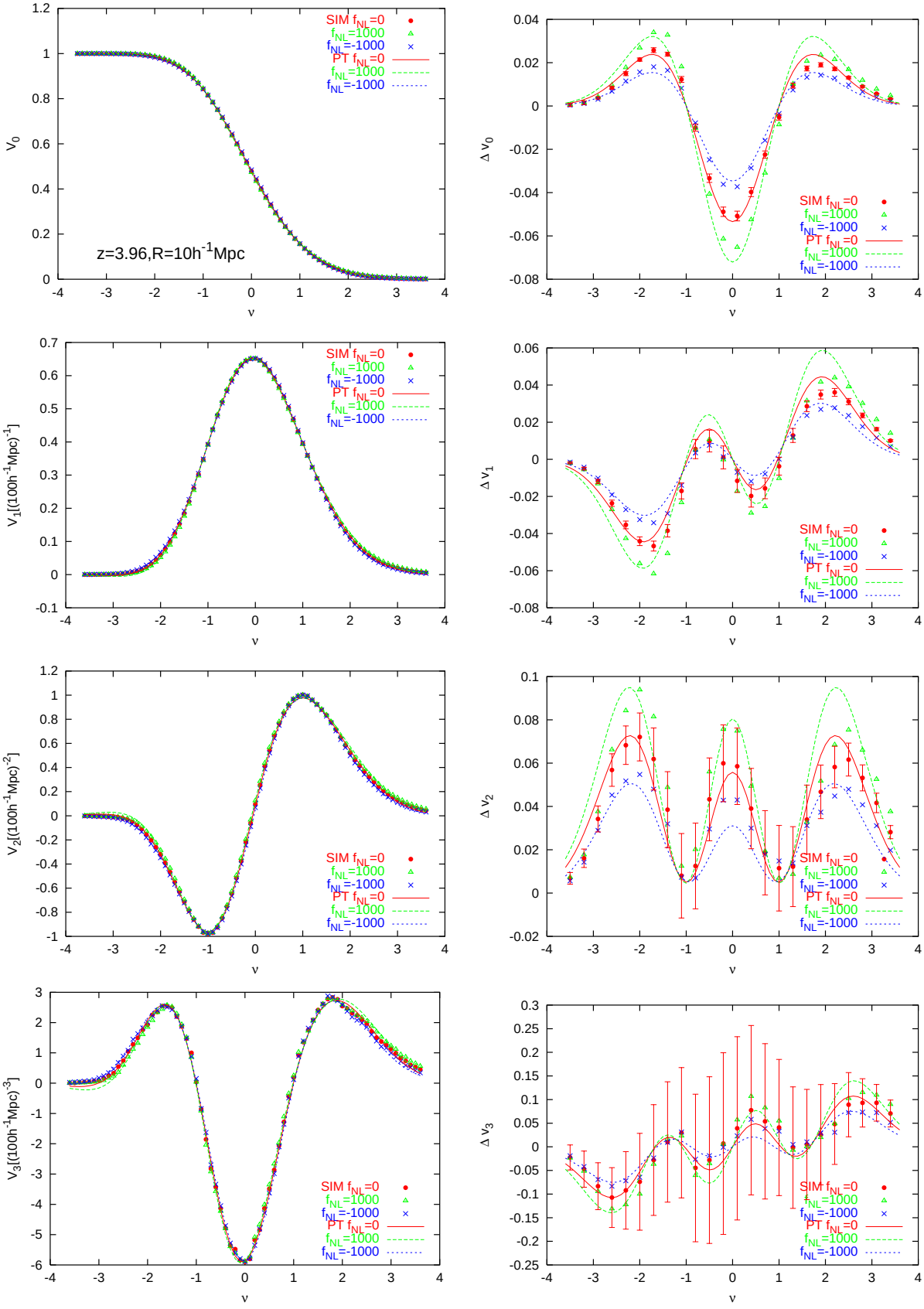

Figure 2. Four Minkowski Functionals V_k (*left*) and their difference ratios Δv_k (*right*) for the simulated mass density fields at $z = 3.96$, with $f_{\rm NL} = 0$ (filled circles), 1000 (open triangles) and -1000 (crosses). The simulated fields are smoothed with a Gaussian window function at the scale $R = 10h^{-1}$Mpc. The error-bars denote the sample variance estimated from 1000 Gaussian realizations with same z, R and box-size as the simulations. For comparison, the theoretical expectations from perturbation theory (equations [2] and [7]) are plotted with lines.

Table 1. Root-mean-square differences between simulated MFs and perturbative formulae at different z and $f_{\rm NL}$ with the corresponding σ_0. The smoothing scale is fixed at $R = 10h^{-1}$Mpc.

z	$f_{\rm NL}$	σ_0	$\sqrt{\langle(\Delta v_k^{\rm (SIM)} - \Delta v_k^{\rm (PT)})^2\rangle}$				$\sqrt{\langle(\Delta v_k^{\rm (SIM)} - \Delta v_k^{\rm (PT)})^2\rangle}/\sqrt{\langle(\Delta v_k^{\rm (SIM)})^2\rangle}$			
			V_0	V_1	V_2	V_3	V_0	V_1	V_2	V_3
5.15	0	0.080	0.003	0.006	0.009	0.024	0.15	0.27	0.24	0.41
5.15	1000	0.080	0.005	0.008	0.013	0.029	0.17	0.27	0.24	0.38
5.15	−1000	0.080	0.003	0.006	0.012	0.024	0.33	0.44	0.40	0.54
3.96	0	0.099	0.003	0.006	0.009	0.023	0.14	0.24	0.20	0.37
3.96	1000	0.099	0.006	0.010	0.014	0.031	0.20	0.34	0.26	0.41
3.96	−1000	0.099	0.003	0.004	0.008	0.020	0.14	0.20	0.23	0.41
2.13	0	0.16	0.007	0.014	0.021	0.044	0.18	0.34	0.29	0.44
2.13	1000	0.16	0.011	0.021	0.029	0.057	0.23	0.40	0.34	0.48
2.13	−1000	0.16	0.004	0.010	0.017	0.034	0.15	0.31	0.27	0.40
0.96	0	0.24	0.015	0.030	0.043	0.081	0.26	0.48	0.41	0.58
0.96	1000	0.24	0.020	0.039	0.055	0.10	0.31	0.54	0.48	0.65
0.96	−1000	0.24	0.010	0.023	0.034	0.065	0.22	0.43	0.36	0.51
0	0	0.38	0.035	0.067	0.095	0.17	0.40	0.68	0.63	0.86
0	1000	0.38	0.042	0.078	0.11	0.19	0.44	0.73	0.69	0.93
0	−1000	0.38	0.028	0.058	0.083	0.15	0.36	0.64	0.58	0.80

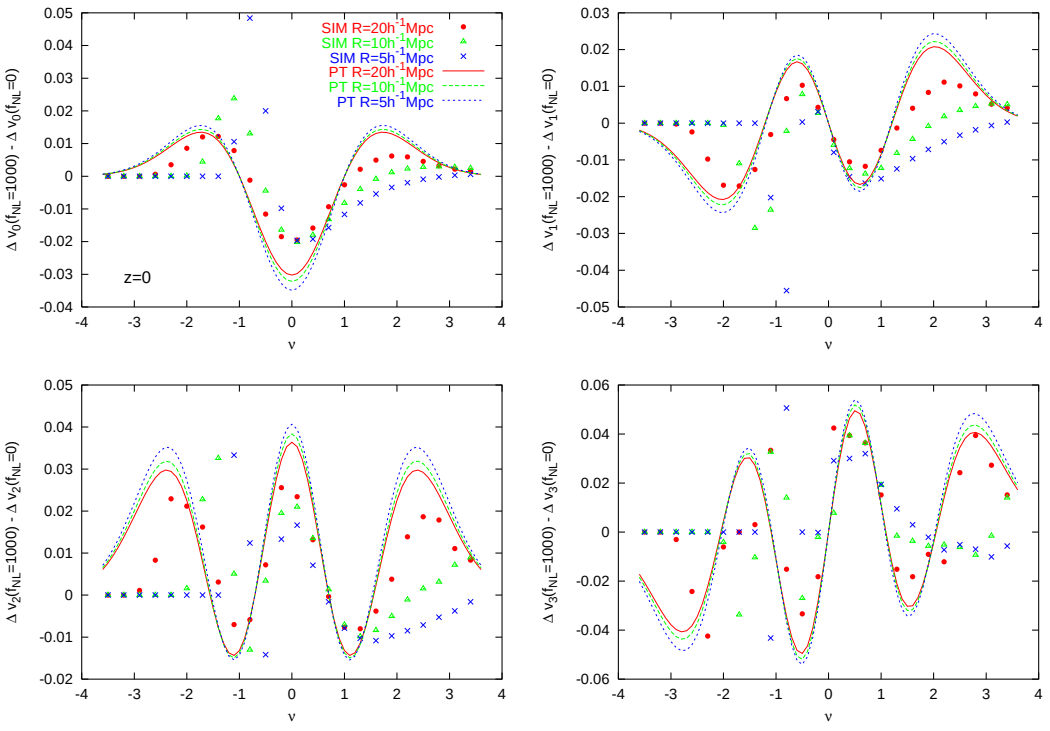

Figure 3. The difference of Δv_k with $f_{\rm NL} = 1000$ from those obtained with Gaussian initial conditions $\Delta v_k(f_{\rm NL} = 0)$ at $z = 0$ for different smoothing scales $R = 20h^{-1}$Mpc ($\sigma_0 = 0.17$), $10h^{-1}$Mpc ($\sigma_0 = 0.38$), and $5h^{-1}$Mpc ($\sigma_0 = 0.74$). Simulated results averaged over three bins are plotted with symbols and the perturbative formulae are also plotted with lines.

also seen quantitatively in Table 1. The shape of the deviation is skewed to the positive side of ν with a higher peak at $\nu = -1/\sigma_0$ (the number density is zero) while the overall amplitude of the deviation Δv_k is roughly the same as that from the perturbative predictions.

It is interesting to estimate the sensitivity of the MFs to primordial non-Gaussianity in the non-linear regime, because the effect of primordial non–Gaussianity on the MFs should become increasingly significant as the sample variance decreases, i.e. at smaller smoothing scales. The MFs are, however, strongly correlated with each other among different bins of the threshold ν and it is therefore necessary to take into account their covariance when estimating the significance of the primordial non-Gaussian effect with, e.g., chi-squared statistics. If the covariances among different bins were not considered, one would overestimate the

value of chi-square as the total number of bins increases. When the field follows nearly Gaussian statistics, the covariance matrix is well approximated with the one numerically estimated from a large number of Gaussian realizations. (Komatsu et al. 2003; Hikage et al. 2006). When the field is non-linearly evolved, it is an exceptionally time-consuming process to generate enough number of realizations to compute the inverse matrix of the covariance (the number of realizations must be larger than the degree-of-freedom at least).

Instead of calculating the covariance matrix directly, therefore, we instead estimate the amount of information contained in each MF as a function of ν. For this purpose, we calculate the effective number of bins $N_{\rm eff}$ for each MF and for all MFs combined as follows:

$$N_{\rm eff} = N_{\rm bin} \frac{\sum_{i,j}^{N_{\rm bin}} \Delta v_i^{\rm (PT)} (C^{-1})_{ij} \Delta v_j^{\rm (PT)}}{\sum_{i}^{N_{\rm bin}} \Delta v_i^{\rm (PT)} C_{ii}^{-1} \Delta v_i^{\rm (PT)}} \quad (19)$$

where i and j denote the binning number of different ν and different kinds of MFs and $N_{\rm bin}$ denotes the total number of bins. The covariance matrix $C_{ij} = \langle \Delta v_i \Delta v_j \rangle$ is computed from 1000 Gaussian realizations with the same cosmological parameters and the same box-size as those of the N-body simulations. As $N_{\rm bin}$ is increased in a fixed range of ν from -3.6 to 3.6, the values of $N_{\rm eff}$ converges to 2, 6, 8, and 12 for each MF from $k = 0$ to 3 and then 12 for all MFs combined. The results indicate that the correlations among different bins of ν is very strong for V_0 and that higher k-th MFs have more independent information as a function of ν.

Applying the value of $N_{\rm eff}$ for non-linearly evolved simulations, we calculate the chi-square values of the primordial non-Gaussian effect on MFs as a function of $f_{\rm NL}$ as

$$\chi^2(f_{\rm NL}) = \frac{N_{\rm eff}}{N_{\rm bin}} \sum_{i}^{N_{\rm bin}} \frac{(\Delta v_i^{\rm (SIM)}(f_{\rm NL}) - \Delta v_i^{\rm (SIM)}(f_{\rm NL}=0))^2}{\langle \Delta v_i^{\rm (SIM)}(f_{\rm NL}=0)^2 \rangle} \quad (20)$$

The variance $\langle \Delta v_i^{\rm (SIM)}(f_{\rm NL}=0)^2 \rangle$ is estimated from 10 realizations of N-body simulations with Gaussian initial conditions (the cosmological parameters and simulation box-size are the same as for the N-body simulations). The normalized MFs $\Delta v_k(f_{\rm NL})$ at arbitrary $f_{\rm NL}$ is linearly interpolated using the simulation results with $f_{\rm NL} = 0$ and 1000. We confirm that the linear interpolation works well using simulations with $|f_{\rm NL}| = 100$ and 500.

Table 2 lists the value of $f_{\rm NL}$ at different R when the effect of the primordial non-Gaussianity is comparable to the sample variance, that is $\chi^2 = 1$. The volume of the simulation box-size is $0.125(h^{-1}{\rm Gpc})^3$, which is less than half the volume of the SDSS main galaxy sample $0.3(h^{-1}{\rm Gpc})^3$. As the smoothing scale decreases, the primordial non-Gaussianity becomes significant. At $R = 5h^{-1}$Mpc, the primordial non-Gaussianity with $f_{\rm NL} = 50$ is comparable to the sample variance and then corresponds to the current observational constraints from WMAP. Note that the detectability of primordial non–Gaussianity from actual observations is, however, strongly dependent on the uncertainty of the cosmological parameters and the galaxy biasing, which we have not attempted to model in detail.

Table 2. The values of $f_{\rm NL}$ at $\chi^2 = 1$ when the effect of the primordial non-Gaussianity is comparable to the sample variance of mass density field for different smoothing scale R (equation [20]). The values of $N_{\rm eff}$ for each MF V_k are 2, 6, 8, and 12 from $k = 0$ to 3 and 12 for all MFs combined. The volume of the density field is a cube at a length $0.5h^{-1}$Gpc and the redshift is 0. The other cosmological parameters are fixed to be fiducial values. The effective number of bins $N_{\rm eff}$ (equation [19]) is also listed in last line.

$R[h^{-1}{\rm Mpc}]$	$f_{\rm NL}$ at $\chi^2 = 1$				
	V_0	V_1	V_2	V_3	All MFs
30	770	480	520	370	350
20	420	300	310	210	210
10	190	180	140	150	110
5	90	80	90	60	50

5 SUMMARY AND CONCLUSIONS

We have studied the imprint of primordial non–Gaussianity on the topological properties of LSS using the MFs. Characterizing primordial non–Gaussianity as a quadratic correction to the primordial potential fluctuation with constant amplitude $f_{\rm NL}$, we compare the MFs with different values of $f_{\rm NL}$ from the mildly to the strongly non-linear regime using high-resolution N-body simulations. Perturbative formulae of the MFs based on the multivariate Edgeworth expansion well reproduce the MFs of simulated mass density fields in the weakly non-linear regime. When the amplitude of the density fluctuation $\sigma_0 < 0.1$ and $|f_{\rm NL}| < 1000$, the deviations of the perturbative formulae from simulations are less than a few percent of the amplitude of each MF. They are also $10 \sim 40$ percent in respect to the non-Gaussian contributions alone.

As the fluctuations become more strongly non-linear, the simulated MFs begin to deviate significantly from the perturbative predictions owing to non-linear gravitational evolution. In order to include small-scale information in realistic cosmological data sets, detailed numerical analysis is therefore essential.

When we include information from smaller scale fluctuations, the effects of primordial non–Gaussianity are indeed significant. Using χ^2 statistics, we find that the primordial non-Gaussianity with $f_{\rm NL} = 50$ has a significance level corresponding to 1σ, considering the sample variance of mass density fields at $R = 5h^{-1}$Mpc with a volume of $0.125(h^{-1}{\rm Gpc})^3$. This implies that measuring the MFs in a SDSS-like survey could constrain $f_{\rm NL}$ at a level comparable with current CMB limits. This is an interesting result, since other observations, like the cluster abundance, that can effectively constrain $f_{\rm NL}$ at high redshifts, become useless at $z = 0$ when non–Gaussian features generated by non-linear dynamics completely obliterate primordial ones (Grossi et al. 2007; Kang et al. 2007).

The actual detectability of the primordial non–Gaussianity is, however, strongly dependent on the degeneracy between the cosmological parameters and the primordial non–Gaussian effect. Understanding the properties of the galaxy biasing is also very important in determining the primordial non–Gaussianity accurately. We will consider this issue in a forthcoming paper.

ACKNOWLEDGMENTS

We thank the anonymous referee for helpful comments. We thank Takahiko Matsubara for useful discussions. C.H. acknowledges support from the Particle Physics and Astronomy Research Council grant number PP/C501692/1. Computations have been performed on the IBM-SP5 at CINECA (Consorzio Interuniversitario del Nord-Est per il Calcolo Automatico), Bologna, with CPU time assigned under an INAF-CINECA grant and on the IBM-SP4 machine at the "Rechenzentrum der Max-Planck-Gesellschaft" at the Max-Planck Institut für Plasmaphysik with CPU time assigned to the MPA. We acknowledge financial contribution from contracts ASI-INAF I/023/05/0, ASI-INAF I/088/06/0 and INFN PD51.

REFERENCES

Alishahiha M., Silverstein E., Tong D., 2004, Phys. Rev. D., 70, 123505
Arkani-Hamed N., Creminelli P., Mukohyama S., Zaldarriaga M., 2004, JCAP, 4, 1
Bardeen J. M., 1980, Phys. Rev. D., 22, 1882
Bartolo N., Komatsu E., Matarrese S., Riotto A., 2004, Phys. Rept., 402, 103
Bartolo N., Matarrese S., Riotto, A., 2002 Phys. Rev. D 65, 103505
Battefeld D., Battefeld T., 2007, JCAP, 5, 1
Bernardeau F., Kofman L., 1995, ApJ, 443, 479
Bernardeau F., Uzan, J.-P., 2002, Phys. Rev. D., 66, 103506
Chen X., Richard E, Eugene A. L., 2007, JCAP, 6, 23
Chodorowski M. J., Bouchet F. R., 1996, MNRAS, 279, 557
Coles P., Davies A. G., Pearson R. C., 1996, MNRAS, 281, 1375
Creminelli P., Nicolis A., Senatore L., Tegmark M., Zaldarriaga M., 2006, JCAP, 0605, 004
Crocce, M., Sebastián, P., Scoccimarro, R., 2006, MNRAS, 373, 369
Dalal N., Doré O., Huterer D., Shirokov, A., 2007, preprint (astro-ph/0710.4560)
Dvali G., Gruzinov A., Zaldarriaga M., 2004, Phys. Rev. D., 69, 083505
Eisenstein, D. J., Hu, W., 1999, ApJ, 511, 5
Fry J.N., Scherrer R.J., 1994, ApJ, 429, 36
Gangui A., Lucchin F., Matarrese S., Mollerach S., 1994, ApJ, 430, 447
Glazebrook K., Eisenstein D., Dey A., Nichol R., & The WFMOS Feasibility Study Dark Energy Team, 2005, preprint (astro-ph/0507457)
Grossi M., Dolag K., Branchini E., Matarrese S., Moscardini L., 2007, preprint (astro-ph/0707.2516)
Hikage C., Schmalzing J., Buchert T., Suto Y., Kayo I., Taruya A., Vogeley M.S., Hoyle F., Gott J.R. III, Brinkmann J., 2003, PASJ, 55, 911
Hikage C., Komatsu E., Matsubara T., 2006, ApJ, 653, 11
Hill G.J., Gebhardt K., Komatsu E., MacQueen, P.J., 2004, in AIP Conf. Proc. 743: The New Cosmology: Conference on Strings and Cosmology, ed. R. E. Allen, D. V. Nanopoulos, & C. N. Pope, 224-233
Kang X., Norberg P., Silk J., 2007, MNRAS, 376, 343
Komatsu E., Spergel D.N., 2001, Phys. Rev. D, 63, 63002
Komatsu E. et al., 2003, ApJS, 148, 119
Lyth D.H., Ungarelli C., Wands D., 2003, Phys. Rev. D., 67, 23503
Matsubara T., 2003, ApJ, 584, 1
Mecke K.R., Buchert T., Wagner H., 1994, A&A, 288, 697
Melnick G.J., Fazio G.G., Tolls V., Jaffe D.T., Gebhardt K., Bromm V., Komatsu E., Woodruff R. A., 2004, Bulletin of the American Astronomical Society, 1509
Nakagami T., Matsubara T., Schmalzing J., Jing Y., 2004, preprint (astro-ph/0408248)
Schmalzing J., Buchert T., 1997, ApJ, 482, L1
Schmalzing J., Górski K.M., 1998, MNRAS, 297, 355
Scoccimarro R., Sefusatti E., Zaldarriaga M., 2004, Phys. Rev. D., 69, 103513
Sefusatti E., Komatsu E., 2007, Phys. Rev. D., 76, 083004
Spergel D.N. et al., 2007, ApJS, 170, 377
Springel V., 2005, MNRAS, 364, 1105
Verde L., Wand L., Heavens A.F., Kamionkowski M., 2000, MNRAS, 313, 141
Watts P.I.R., Coles P., 2003, MNRAS, 338, 806